**Letter**

# Solvable model for discrete time crystal enforced by nonsymmorphic dynamical symmetry

Zi-Ang Hu [1], Bo Fu,[1] Xiao Li,[2,3] and Shun-Qing Shen [1,*]

[1]*Department of Physics, The University of Hong Kong, Pokfulam Road, Hong Kong, China*
[2]*Department of Physics, City University of Hong Kong, Kowloon, Hong Kong, China*
[3]*City University of Hong Kong Shenzhen Research Institute, Shenzhen 518057, Guangdong, China*

Discrete time crystal is a class of nonequilibrium quantum systems exhibiting subharmonic responses to external periodic driving. Here we propose a class of discrete time crystals enforced by nonsymmorphic dynamical symmetry. We start with a system with nonsymmorphic dynamical symmetry, in which the instantaneous eigenstates become Möbius twisted, hence doubling the period of the instantaneous state. The exact solution of the time-dependent Schrödinger equation shows that the system spontaneously exhibits a period expansion without undergoing quantum superposition states for a series of specific evolution frequencies or in the limit of a long evolution period. In this case, the system gains a $\pi$ Berry phase after two periods' evolution. While the instantaneous energy state is subharmonic to the system, the interaction will trigger off decoherence and thermalization that stabilize the oscillation pattern.

*Introduction.* Recently, the spontaneous breaking of time translation symmetry has attracted tremendous attention and led to the idea of time crystal [1]. Although it has been shown that no system can spontaneously break the continuous time translation symmetry [2], it is possible to break the discrete time translation symmetry in Floquet quantum many-body systems [3–14]. This new nonequilibrium phase has since been verified in a series of experiments [15–22]. Subsequent studies in nonequilibrium Floquet quantum systems further generalize to incorporate both spatial and temporal dimensions, giving rise to a wide range of new phenomena, including the space-time crystals [23–27]. In particular, it has been shown that a nonsymmorphic symmetry can enforce energy band crossings and create a Möbius twist as well as additional topological properties [27–33]. It remains unclear what will happen when a system hosts nonsymmorphic *dynamical* symmetry.

Here we propose a class of discrete time crystals (DTCs) enforced by the nonsymmorphic dynamical symmetry. We reveal the dynamic behavior of such systems by presenting an exact solution to the time-dependent evolution of a two-level system. The instantaneous eigenstates of the system are Möbius twisted when the nonsymmorphic dynamical symmetry is present. The exact time-dependent solution shows that the quantum states of the system embrace evolution along the twisted instantaneous state so that the period of the states is doubled to that of the system Hamiltonian when the ratio

between the width of the instantaneous energy band to the evolution frequency of the system's Hamiltonian equals a set of discrete values, or when the system evolves in the long-period limit. In addition, the system has a nontrivial topology with a half-integer winding number and a $\pi$ Berry phase in two cycles of evolution. Also, we explore the system's stability in the presence of interactions and show the robustness of this class of DTCs. The exact solution provides explicit evidence to support the spontaneous breaking of the time translation symmetry in discrete time crystals.

*Model with a Möbius twist in instantaneous state.* The nonsymmorphic dynamical symmetry operation represents a unique category of symmetry operations that integrates both spatial transformations and nontrivial time translation operations, which cannot be performed independently. When nonsymmorphic symmetry is incorporated, the resulting extension of the symmetry group exhibits topologically nontrivial properties, leading to intriguing characteristics in group representations. In the realm of group representation theory, the instantaneous state of the system adheres to the irreducible representation of the symmetry group, while the Hamiltonian aligns with the induced representation of the nonsymmorphic symmetry. When the symmetry exhibits nonsymmorphic symmetry, the period of the irreducible representation does not consistently align with the period of the induced representation. Consequently, this inconsistency generates a mismatch between the periods of the instantaneous state and the Hamiltonian.

Specifically, we start with a time-dependent two-level Hamiltonian with the dynamical glide symmetry [29],

$$H_0(t) = \frac{1}{2}\hbar\Omega\sin(\omega t)\sigma_x + \hbar\Omega\sin^2\left(\frac{\omega t}{2}\right)\sigma_y, \quad (1)$$

where $\sigma_i$ $(i = x, y, z)$ are the Pauli matrices. The Hamiltonian has a period of $T = \frac{2\pi}{\omega}$. At time $t$, the instantaneous
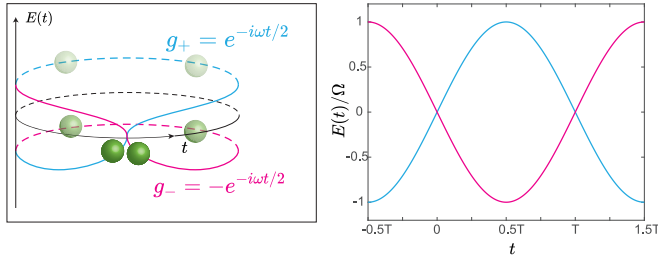
FIG. 1. Illustration of Möbius twist of the instantaneous state and evolution process of DTC. The red and blue lines label different eigenstates of the symmetry operator $G$. The vertical direction shows the relativity energy of two states. The two eigenstates will swap after one period of evolution and go back to themselves after two periods. The green ball represents the quantum states' evolution which will go into a superposition state of instantaneous states (translucent balls) and go to another instantaneous state after one period evolution.

eigenstates are $\phi_\chi(t) = \frac{1}{\sqrt{2}}[\chi e^{-i\omega t/2}, 1]^{\mathsf{T}}$ ($\mathsf{T}$ indicates the transpose), with $\chi = \pm 1$. The corresponding energy eigenvalues are $E_\chi(t) = \chi\hbar\Omega\sin(\omega t/2)$. The model possesses a nonsymmorphic dynamical symmetry $\tilde{g}$, the square of which will be a time translation symmetry with one period. The matrix representation of $\tilde{g}$ in the basis of the two-level system is the reduced representation of the whole group and has the following form:

$$G(t) = \begin{pmatrix} 0 & e^{-i\omega t} \\ 1 & 0 \end{pmatrix}. \tag{2}$$

As a result, the Hamiltonian commutes with $G(t)$, $[H(t), G(t)] = 0$. Because $G(t)$ is the induced representation, it has the same period $T$ as the Hamiltonian, $G(t + T) = G(t)$. Furthermore, $G^2(t) = e^{-i\omega t}$ is the irreducible representation of the time translation symmetry with a period $T$. Consequently, the eigenvalues of $G(t)$ are $g_\chi(t) = \chi e^{-i\omega t/2}$. The corresponding eigenstates are the instantaneous eigenstates of the system, $\phi_\chi(t)$. The eigenvalues $g_\chi(t)$ are in the irreducible representations of the extended symmetry group whose period is twice that of the system's period. In addition, it has the swapping property within one period as $g_\chi(t + T) = g_{-\chi}(t)$ and $g_\chi(t + 2T) = g_\chi(t)$. The corresponding eigenstates $\phi_\chi(t)$ share the same property. The swapping property of the eigenvalues and eigenstates is a manifestation of the group monodromy. It directly illustrates the periodic extension by introducing the nonsymmorphic symmetry. Another consequence of this period mismatch is that the instantaneous eigenstates of the system automatically become Möbius twisted. Figure 1 illustrates how the Möbius twist happens. The two colored lines represent the two eigenstates of the symmetry operator $G(t)$, which are also the instantaneous eigenstates of the Hamiltonian. After one cycle of evolution, the two eigenstates will swap. Since the instantaneous eigenstates of the Hamiltonian still host the discrete time translation symmetry, it is forced to undergo a symmetry-enforced crossing in the evolution process. The two eigenstates are Möbius twisted at $t = T$ such that they only come back to themselves after a two-period evolution, matching the period of the irreducible representation of the symmetry group.

Besides period doubling in the two-level system with a dynamical glide symmetry, systems with other nonsymmorphic symmetry can also have other ways of period expansion. For example, dynamical screw symmetry in multilevel systems allows the period expansion of more than two (see Supplemental Material [34]).

*Exact solution and DTC.* The exact solution $\Psi(t)$ of the time-dependent Hamiltonian in Eq. (1) can be obtained by solving the time-dependent Schrödinger equation, $i\hbar\partial_t\Psi(t) = H_0(t)\Psi(t)$. In the basis of the instantaneous eigenstates $\phi_\chi(t)$, an ansatz for the time-dependent solution is $\Psi(t) = \sum_\chi c_\chi(t)\exp[i\frac{\omega t}{4} - \frac{i}{\hbar}\int_0^t E_\chi(t')dt']\phi_\chi(t)$, where $c_\chi(t)$ are two time-dependent coefficients. Substituting the wave function into the time-dependent Schrödinger equation, we find that $c_\chi(t)$ satisfies

$$\partial_x^2 c_\chi - i\chi\alpha\sin(2x)\partial_x c_\chi + c_\chi = 0, \tag{3}$$

where $x = \frac{\omega t}{4}$ and $\alpha = \frac{8\Omega}{\omega}$. Note that $c_\chi(t)$ depend on $\chi$, $\alpha$, and $x$. We denote the initial state as $\Psi(0) = \sum_\chi c_\chi(0)\phi_\chi(0)$, with $c(x) \equiv [c_+(x), c_-(x)]^{\mathsf{T}}$. The solutions for $c_\chi(t)$ are found as follows:

$$c(x) = \begin{pmatrix} H_c^+(\alpha, x) & -i\sin(x)H_c^-(\alpha, x) \\ -i\sin(x)H_c^-(\alpha, x)^* & H_c^+(\alpha, x)^* \end{pmatrix} c(0). \tag{4}$$

Here we define

$$H_c^\chi(\alpha, x) \equiv H_c\left(i\alpha, -\frac{\chi}{2}, -\frac{1}{2}, -\frac{i\alpha}{2}, \frac{1}{8} + \frac{i\alpha}{4}; \sin^2 x\right), \tag{5}$$

where $H_c$ is the confluent Heun function [35,36], which satisfies the boundary conditions $H_c^\chi(\alpha, x = 0) = 1$ and $\frac{d}{dx}H_c^\chi(\alpha, x)|_{x=0} = 0$. The complex conjugate of Eq. (3) requires that $H_c^\chi(-\alpha, x) = H_c^\chi(\alpha, x)^*$. Assuming the initial state is the eigenstate of $\sigma_x$ with eigenvalue $\chi = +1$, i.e., $c_+(0) = 1$ and $c_-(0) = 0$, we have $c_+(x) = H_c^+(\alpha, x)$ and $c_-(x) = -i\sin x H_c^-(-\alpha, x)$. The wave-function normalization further requires that $|H_c^+(\alpha, x)|^2 + \sin^2(x)|H_c^-(\alpha, x)|^2 = 1$.

The solution in Eq. (4) reveals a subharmonic behavior of dynamical evolution to the $H(t)$ at a series of the specific ratio $\alpha$, i.e.,

$$\Psi(t + 2T) = -\Psi(t), \tag{6}$$

which is a hallmark feature of a DTC. Although the instantaneous eigenstates are Möbius twisted and only return to themselves after $2T$, the quench dynamics starting from a generic initial state usually does not follow the same behavior. To analyze this question, we introduce the time evolution operator $U(t)$, which satisfies $\Psi(t) = U(t)\Psi(0)$. By comparing the initial condition $c_\chi(0) = \phi_\chi^\dagger(0)\Psi(0)$ with the exact solution in Eq. (4), we can obtain the general expression for the time evolution operator $U(t)$ (see Supplemental Material [34]). Consider the initial state $\phi_+(0)$. After one period $t = T$ or $x \equiv \frac{\omega T}{4} = \frac{\pi}{2}$, the probability that the system still stays in the initial state is given by

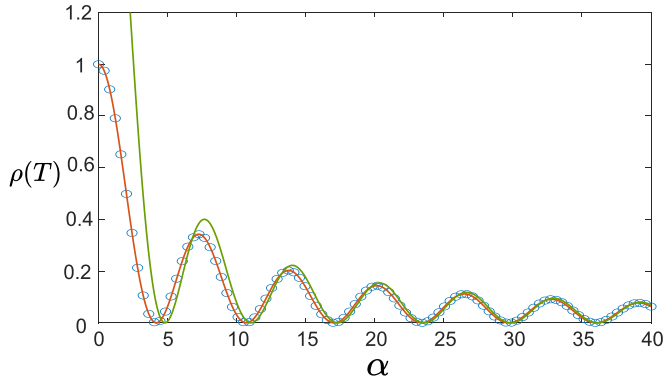$$\rho(T) = |\phi_+^\dagger(0)U(T)\phi_+(0)|^2 = \left|H_c^-\left(\alpha_n, \frac{\pi}{2}\right)\right|^2.$$

FIG. 2. The remaining probability $\rho(T)$ after one period evolution with different value of $\alpha$. The red line is the $H_c^-(\alpha, \frac{\pi}{2})$, the green line is $\frac{\pi}{2}J_0(\frac{\alpha}{2})$ working as an asymptotic approximation, and the blue dots are the value of numerical methods.

Specifically, $H_c^-(\alpha, \frac{\pi}{2})$ has an oscillatory decay with $\alpha$, and drops to zero for several $\alpha = \alpha_n$, $H_c^-(\alpha_n, \frac{\pi}{2}) = 0$, as shown in Fig. 2. According to the normalization condition, the other Heun function satisfies $|H_c^+(\alpha_n, \frac{\pi}{2})| = 1$. Hence, we can write $H_c^+(\alpha_n, \frac{\pi}{2}) \equiv \exp[i\theta_n]$. The first 10 $\alpha_n$ and $\theta_n$ are listed in Table I. For a large $n$, $\alpha_n \simeq 2n\pi - \frac{\pi}{2}$ and $\theta_n \simeq \frac{\pi}{\alpha_n}$. Consequently, we have $c_\pm(\frac{\pi}{2}) = \exp[\pm i\theta_n]c_\pm(0)$, indicating that the coefficients gain extra phases in one period of evolution. This result shows that the state does not return to the initial one. In this case, the time evolution operator has the form of

$$U_n(T) = -i\sigma_z e^{-i\sigma_x \left(\frac{\alpha_n}{2} - \theta_n\right)} \quad (7)$$

for specific values of $\alpha = \alpha_n$. For $t = 2T$, it follows that $U_n(2T) = -1$. Thus, after a two-period evolution, the quantum state will return to its initial state and gains a $\pi$ Berry phase, as shown in Eq. (6). This manifests the presence of the DTC.

When the period is long ($\alpha \gg 1$), we can approximate the confluent Heun function by the zeroth Bessel function, $H_c^-(\alpha, \frac{\pi}{2}) \simeq e^{i\frac{\alpha}{2}} \frac{\pi}{2} J_0(\frac{\alpha}{2})$, as shown in Fig. 2. The time evolution operator then has the form

$$U(T) \simeq \left[ -i\sqrt{1 - \frac{\pi^2}{4} J_0^2\left(\frac{\alpha}{2}\right)} \sigma_z + e^{i\frac{\alpha}{2}} \frac{\pi}{2} J_0\left(\frac{\alpha}{2}\right) \right] e^{-i\sigma_x \left(\frac{\alpha}{2} - \frac{\pi}{\alpha}\right)}. \quad (8)$$

If the initial state is one of the eigenstates of $\sigma_x$, say $\phi_+(0)$, the state will mainly evolve into the other eigenstate $\phi_-(0)$,

TABLE I. The numerical value of the first 10 $\alpha_n$ of the Heun function and the phase factor $\theta_n$. With $n \to \infty$, they have asymptotic behavior as $\alpha_n \simeq 2\pi n - \frac{\pi}{2}$ and $\theta_n \simeq \frac{\pi}{\alpha_n}$.

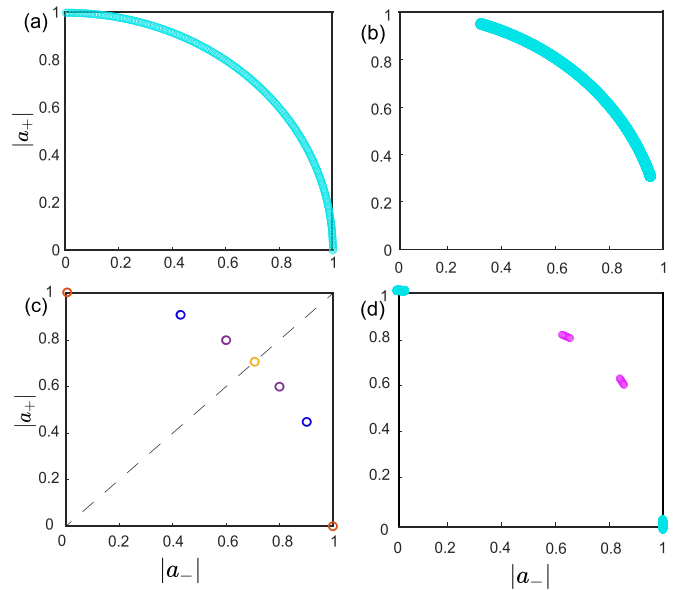| $n$ | 1 | 2 | 3 | 4 | 5 | 6 | 7 |
|---|---|---|---|---|---|---|---|
| $\alpha_n$ | 4.21 | 10.73 | 17.11 | 23.44 | 29.75 | 36.07 | 42.36 |
| $\theta_n$ | 0.391 | 0.199 | 0.138 | 0.108 | 0.0889 | 0.0756 | 0.0664 |
| $n$ | 8 | 9 | 10 | 11 | 12 | 13 | 14 |
| $\alpha_n$ | 48.66 | 54.95 | 61.24 | 67.46 | 73.76 | 80.07 | 86.34 |
| $\theta_n$ | 0.0592 | 0.0535 | 0.0483 | 0.0459 | 0.0424 | 0.0396 | 0.0371 |



FIG. 3. The stroboscopic projection values in the first 300 periods. (a) The projections values at $\alpha = 8$ (not one of $\alpha_n$) for the initial state $(1, 0)^\mathsf{T}$, indicating no sign of periodicity in the time evolution. (b) The projection values at $\alpha = 8$ for $(0.6, 0.8)^\mathsf{T}$. (c) The projection values at $\alpha = \alpha_3 = 17.11$. The different color paired points indicate, for the different initial states, $(1, 0)^\mathsf{T}$ (red), $(0.6, 0.8)^\mathsf{T}$ (purple), $(0.90, 0.436)^T$ (blue), and $(\sqrt{2}/2, \sqrt{2}/2)^\mathsf{T}$. (d) The projection values at $\alpha = 80$ (large, but not one of $\alpha_n$). The initial state: $(1, 0)^\mathsf{T}$(blue) and $[0.6, 0.8]^\mathsf{T}$(pink).

and the probability to stay in the state $\phi_+(0)$ is just $\rho(T)$. Interestingly, the energy crossing here invalidates the adiabatic theorem. Furthermore, after a two-period evolution, we have $U(2T) \simeq -1$. In this limit, the system is still approximately a DTC even if $\alpha$ is not equal to $\alpha_n$.

To illustrate the periodicity of the evolution of the quantum state, we project the state $\Psi(t = nT) \equiv U(nT)\Psi(0)$ onto the two basis states $\phi_\chi(0)$, where $n$ is a positive integer. We denote the two resulting projection parameters as $a_\pm(n) = |\langle\phi_\pm(0)|\Psi(nT)\rangle|$, which satisfies $a_+^2(n) + a_-^2(n) = 1$ because of the wave-function normalization. Consequently, the points $[a_+(n), a_-(n)]$ should all locate on a quarter circle with a unit radius. The results for different values of $\alpha$ and the initial states are plotted in Fig. 3. For general $\alpha$ and initial states, the time evolution of the state does not exhibit any periodicity since all quantum states will be visited as $n$ increases. The points $[a_+(n), a_-(n)]$ are expected to fill the entire quarter circle, indicating ergodicity for an arbitrary initial state, as shown in Fig. 3(a). We also find that there are limitations to the ergodicity because a portion of states near the axis will not be visited for some specific initial states and the value of $\alpha$ after a large number $n$ periods of evolution, as shown in Fig. 3(b). However, for $\alpha = \alpha_n$, we note that $\Psi(t = nT)$ have just two states: $\Psi(t = nT) = \pm\Psi(0)$ for an even $n$, and $\Psi(t = nT) = \pm U(T)\Psi(0)$ for an odd $n$. The state $\Psi(t = nT)$ just bounces back and forth between $\Psi(0)$ and $U(T)\Psi(0)$, as shown in Fig. 3(c). The period of the state becomes $2T$, indicating the formation of a DTC. If the initial state happens to be one of the eigenstates of $U(T)$, we have $U(T)\Psi(0) \propto \Psi(0)$.
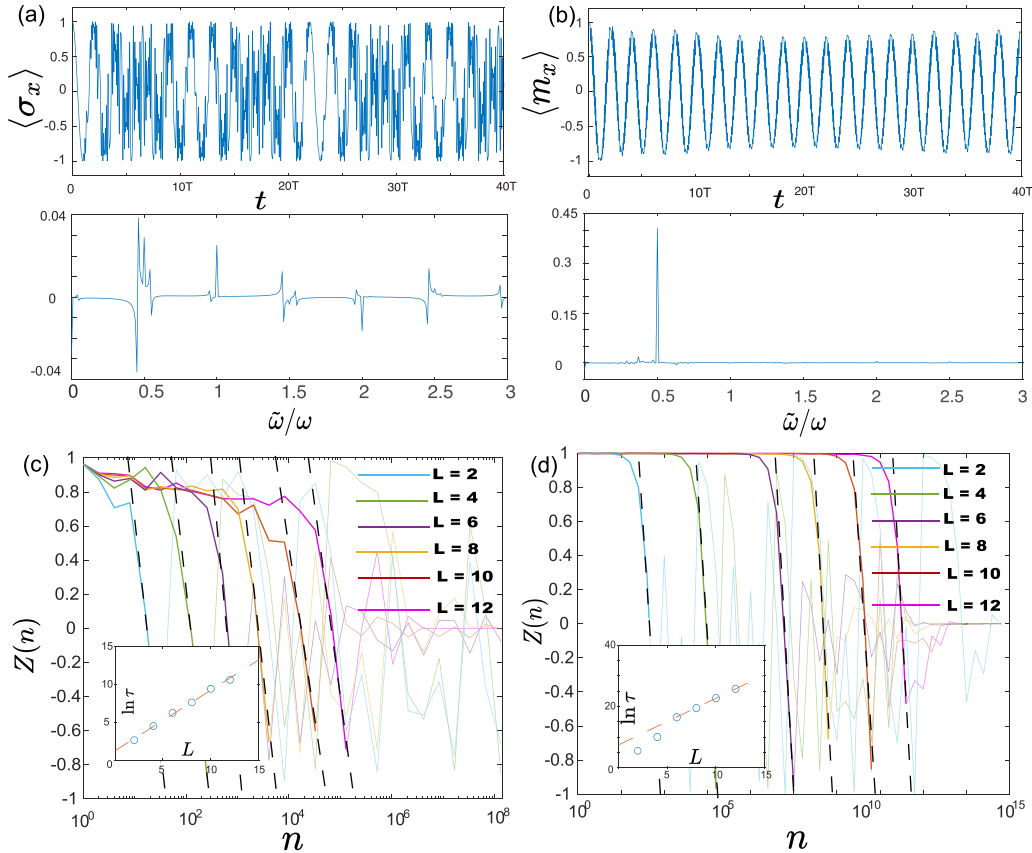
FIG. 4. (a) $\langle\sigma_x(t)\rangle$ and its Fourier spectrum for noninteracting system for the first 40 periods. (b) $\langle m_x(t)\rangle$ and its Fourier spectrum for the interacting system in the $x$ direction with an initial state polarized in the $x$ direction with length $L = 10$. (c) $Z(n)$ at the stroboscopic time, with different length chains showed in the legend. The inset shows the lifetime via the size $L$ of the system. $\tau \propto \exp(bL)$, with $b = 1.56$ for $\alpha = 81.60$ (slightly deviated from $\alpha_{13} = 80.07$). (d) $Z(n)$ at the stroboscopic time for $\alpha = \alpha_{13}$. $b = 2.49$. Here we set the interaction $J = 0, 2\hbar\omega$.

The evolution period is the same as that of the Hamiltonian. In this case, the time translation symmetry is respected. For $\alpha$ slightly deviating from the $\alpha_n$ or $\alpha \gg 1$, as shown in Fig. 3(d), the system approximately keeps the two-period oscillation for a relatively long time.

*Stability of the DTC.* Upon deviating from the $\alpha_n$, the quantum states no longer return to their initial state after two cycles of evolution, causing the off-diagonal term of $\sigma_x$ to dominate and inevitably leading to the dynamical chaos of relevant observables. As illustrated in Fig. 4(a), we depict $\langle\sigma_x(t)\rangle = \langle\Psi(t)|\sigma_x|\Psi(t)\rangle$ for the noninteracting model when $\alpha$ diverges from $\alpha_n$. Notably, the off-diagonal term of $\sigma_x$ in the instantaneous state basis can be represented as

$$\langle\phi_{+1}|\sigma_x|\phi_{-1}(t)\rangle = e^{-i\alpha\sin^2\frac{\omega t}{4}}\sin\frac{\omega t}{2}. \qquad (9)$$

With a significantly large $\alpha$, the dynamical phase factor $e^{-i\alpha\sin^2\frac{\omega t}{4}}$ prompts rapid oscillation in the observable quantity $\langle\sigma_x(t)\rangle$. Furthermore, multiple peaks emerge in the Fourier spectrum of $\langle\sigma_x(t)\rangle$. Thus, no time translation symmetry is respected in this case.

We demonstrate that incorporating many-body interactions can stabilize the subharmonic response, thereby achieving a prethermal DTC. This prethermal DTC is expected to endure in the thermodynamic limit and exhibit robustness against perturbations and imperfect single-spin driving fields. Specifically, we consider a spin chain by comprising multiple identical Floquet two-level spin systems with uniform nearest-neighbor Ising couplings. The Hamiltonian can be expressed as

$$H(t) = H_0(t) + J\sum_i \sigma_\mu^i\sigma_\mu^{i+1}, \qquad (10)$$

with $H_0(t)$ given by Eq. (10) and $J$ representing the Ising interaction between nearest-neighbor sites, $\sigma_\mu^i$ denoting the spin operator of the $i$th site, and $\mu$ taking the values of $x$, $y$, or $z$. We assume that the interaction strength $J$ is considerably smaller than the driving term, such that $|J| \ll \hbar\Omega$. This interaction induces decoherence and thermalization of the Floquet system [37,38]. If the system initiates in one of the instantaneous eigenstates of $H_0(t)$, decoherence among subsystems suppresses the rapid oscillation caused by off-diagonal terms, resulting in a smoother oscillation pattern. To demonstrate the interaction's impact, we assess the average value of $\sigma_x^i$ for all sites, i.e., $\langle m_x(t)\rangle = \frac{1}{N}\sum_i\langle\sigma_x^i(t)\rangle$, and display the oscillation of $\langle m_x(t)\rangle$ over the initial 40 periods. Considering Ising interactions at direction $\mu = x$, we find that the model exhibits a persistent oscillation with a $2T$ period in both cases, even when $\alpha$ deviates from $\alpha_n$. We also exhibit more results with more parameters and longer time behavior.

The DTC reinforced by nonsymmorphic symmetry is resilient to various initial states and site-resolved measurements (see Supplemental Material [34]). The oscillation's Fourier spectrum also presents an isolated peak at $\frac{\omega}{2}$ in Fig. 4(b). This explicitly substantiates the existence of the DTC phase in the presence of the interaction. To further verify that the system constitutes a prethermal DTC, we evaluate the finite-scaling behavior of $\langle m_x(t) \rangle$ at stroboscopic time $t = nT$ ($n$ is an integer), defined as $\langle m_x(nT) = (-1)^n Z(n)$, with the initial state polarized in the $x$ direction, and present the results for different lengths in Fig. 4(c). The calculated $Z(n)$ show that it drops to $\sim$0.8–0.9 and maintains for a short time before starting to drop drastically to around zero, which allows us to define the lifetime $\tau = n_c T$ for the DTC with certain length and parameters. The inset of Fig. 4(c) illustrates that the lifetime $\tau$ grows with the size $L$ of the system in an exponential law. This characteristic is a key feature of a prethermal DTC with spontaneously broken symmetry [3]. Remarkably, the interaction preserves the DTC phase even when the symmetry is slightly disrupted by a minor symmetry breaking perturbation term. For comparison, we also present the lifetime and finite scaling for $\alpha = \alpha_{13}$ in Fig. 4(d). It is noted that the stability of $\langle m_x(t) \rangle$ and the lifetime of the DTC are enhanced drastically for one $\alpha_n$. Thus the interacting multiple Floquet spin system is a prethermal DTC for $\alpha = \alpha_n$ and even for $\alpha$ deviating slightly from $\alpha_n$ in the case of interaction.

*Discussion.* In the previous section, we demonstrated that nonsymmorphic symmetry enforces the instantaneous state into a Möbius twist, resulting in the period-doubled evolution. This period expansion is attributed to the realization of a DTC. The Hamiltonian in Eq. (1) possesses an additional chiral symmetry, defined as $\Gamma = \sigma_z$, such that $\{\Gamma, H\} = 0$. The topological property of the system can be characterized by the winding number, defined as $\nu = \int \frac{dk}{2\pi}(h_y \partial_t h_x - h_x \partial_t h_y)$, if we decompose the Hamiltonian into Pauli matrices as $H = \boldsymbol{h} \cdot \sigma$. When the instantaneous energy bands exhibit a single crossing, the winding number becomes a half integer [29]. This unique winding number is intimately connected to the system's period expansion.

In contrast to gapped systems where the adiabatic theorem applies, the quantum state of the DTC returns to its initial state after two periods, acquiring an extra $\pi$ Berry phase when the frequency equals certain values or in the long-period limit. Experimentally, a DTC quantum simulation can be performed using qubits in a quantum computer, such as quantum superconducting and nuclear magnetic resonance systems [22,39–41]. These systems enable spin manipulation for arbitrary Hamiltonians. The period extension can be directly measured by monitoring the corresponding observable quantities. Additionally, the unique Berry phase can also be measured in these systems. By selecting an initial state polarized in the $x$ direction, the $\pi$ Berry phase can be measured from the $2T$ periodic oscillation of $\langle \sigma_x \rangle$ when $\alpha = \alpha_n$ or in the long-period limit.

[1] F. Wilczek, Quantum Time Crystals, Phys. Rev. Lett. **109**, 160401 (2012).

[2] H. Watanabe and M. Oshikawa, Absence of Quantum Time Crystals, Phys. Rev. Lett. **114**, 251603 (2015).

[3] D. V. Else, B. Bauer, and C. Nayak, Floquet Time Crystals, Phys. Rev. Lett. **117**, 090402 (2016).

[4] D. V. Else, B. Bauer, and C. Nayak, Prethermal Phases of Matter Protected by Time-Translation Symmetry, Phys. Rev. X **7**, 011026 (2017).

[5] K. Sacha, Modeling spontaneous breaking of time-translation symmetry, Phys. Rev. A **91**, 033617 (2015).

[6] K. Sacha and J. Zakrzewski, Time crystals: A review, Rep. Prog. Phys. **81**, 016401 (2017).

[7] N. Y. Yao, A. C. Potter, I.-D. Potirniche, and A. Vishwanath, Discrete Time Crystals: Rigidity, Criticality, and Realizations, Phys. Rev. Lett. **118**, 030401 (2017).

[8] N. Y. Yao, C. Nayak, L. Balents, and M. P. Zaletel, Classical discrete time crystals, Nat. Phys. **16**, 438 (2020).

[9] A. Russomanno, F. Iemini, M. Dalmonte, and R. Fazio, Floquet time crystal in the Lipkin-Meshkov-Glick model, Phys. Rev. B **95**, 214307 (2017).

[10] A. Shapere and F. Wilczek, Classical Time Crystals, Phys. Rev. Lett. **109**, 160402 (2012).

[11] H. Taheri, A. B. Matsko, L. Maleki, and K. Sacha, All-optical dissipative discrete time crystals, Nat. Commun. **13**, 848 (2022).

[12] F. M. Surace, A. Russomanno, M. Dalmonte, A. Silva, R. Fazio, and F. Iemini, Floquet time crystals in clock models, Phys. Rev. B **99**, 104303 (2019).

[13] P. Liang, R. Fazio, and S. Chesi, Time crystals in the driven transverse field Ising model under quasiperiodic modulation, New J. Phys. **22**, 125001 (2020).

[14] A. Pizzi, J. Knolle, and A. Nunnenkamp, Higher-order and fractional discrete time crystals in clean long-range interacting systems, Nat. Commun. **12**, 2341 (2021).

[15] S. Choi, J. Choi, R. Landig, G. Kucsko, H. Zhou, J. Isoya, F. Jelezko, S. Onoda, H. Sumiya, V. Khemani, C. von Keyserlingk, N. Y. Yao, E. Demler, and M. D. Lukin, Observation of discrete time-crystalline order in a disordered dipolar many-body system, Nature (London) **543**, 221 (2017).

[16] P. Jurcevic, H. Shen, P. Hauke, C. Maier, T. Brydges, C. Hempel, B. P. Lanyon, M. Heyl, R. Blatt, and C. F. Roos, Direct Observation of Dynamical Quantum Phase Transitions in an Interacting Many-Body System, Phys. Rev. Lett. **119**, 080501 (2017).

[17] J. Rovny, R. L. Blum, and S. E. Barrett, Observation of Discrete-Time-Crystal Signatures in an Ordered Dipolar Many-Body System, Phys. Rev. Lett. **120**, 180603 (2018).

[18] J. Zhang, P. W. Hess, A. Kyprianidis, P. Becker, A. Lee, J. Smith, G. Pagano, I.-D. Potirniche, A. C. Potter, A. Vishwanath *et al.*, Observation of a discrete time crystal, Nature (London) **543**, 217 (2017).

[19] O. Neufeld, D. Podolsky, and O. Cohen, Floquet group theory and its application to selection rules in harmonic generation, Nat. Commun. **10**, 405 (2019).

[20] A. Kyprianidis, F. Machado, W. Morong, P. Becker, K. S. Collins, D. V. Else, L. Feng, P. W. Hess, C. Nayak, G. Pagano, N. Y. Yao, and C. Monroe, Observation of a prethermal discrete time crystal, Science **372**, 1192 (2021).

[21] B. Wang, J. Quan, J. Han, X. Shen, H. Wu, and Y. Pan, Observation of photonic topological Floquet time crystals, Laser Photon. Rev. **16**, 2100469 (2022).

[22] P. Frey and S. Rachel, Realization of a discrete time crystal on 57 qubits of a quantum computer, Sci. Adv. **8**, eabm7652 (2022).

[23] S. Xu and C. Wu, Space-Time Crystal and Space-Time Group, Phys. Rev. Lett. **120**, 096401 (2018).

[24] Q. Gao and Q. Niu, Floquet-Bloch Oscillations and Intraband Zener Tunneling in an Oblique Spacetime Crystal, Phys. Rev. Lett. **127**, 036401 (2021).

[25] Y. Peng, Topological Space-Time Crystal, Phys. Rev. Lett. **128**, 186802 (2022).

[26] J. Smits, L. Liao, H. T. C. Stoof, and P. van der Straten, Observation of a Space-Time Crystal in a Superfluid Quantum Gas, Phys. Rev. Lett. **121**, 185301 (2018).

[27] K. Giergiel, A. Kuroś, A. Kosior, and K. Sacha, Inseparable Time-Crystal Geometries on the Möbius Strip, Phys. Rev. Lett. **127**, 263003 (2021).

[28] L. Michel and J. Zak, Connectivity of energy bands in crystals, Phys. Rev. B **59**, 5998 (1999).

[29] B. Fu, J.-Y. Zou, Z.-A. Hu, H.-W. Wang, and S.-Q. Shen, Quantum anomalous semimetals, npj Quantum Mater. **7**, 94 (2022).

[30] Y. X. Zhao and A. P. Schnyder, Nonsymmorphic symmetry-required band crossings in topological semimetals, Phys. Rev. B **94**, 195109 (2016).

[31] S.-L. Zhang and Q. Zhou, Two-leg Su-Schrieffer-Heeger chain with glide reflection symmetry, Phys. Rev. A **95**, 061601(R) (2017).

[32] K. Shiozaki, M. Sato, and K. Gomi, $Z_2$ topology in nonsymmorphic crystalline insulators: Möbius twist in surface states, Phys. Rev. B **91**, 155120 (2015).

[33] J. Höller and A. Alexandradinata, Topological Bloch oscillations, Phys. Rev. B **98**, 024310 (2018).

[34] See Supplemental Material at http://link.aps.org/supplemental/10.1103/PhysRevResearch.5.L032024 for a detailed discussion.

[35] K. Heun, The theory of Riemannian functions of second order with four branch points, Math. Ann. **33**, 161 (1888).

[36] F. W. Olver, D. W. Lozier, R. F. Boisvert, and C. W. Clark, *NIST Handbook of Mathematical Functions* (Cambridge University Press, Cambridge, 2010).

[37] A. Haldar, R. Moessner, and A. Das, Onset of Floquet thermalization, Phys. Rev. B **97**, 245122 (2018).

[38] D. A. Abanin, E. Altman, I. Bloch, and M. Serbyn, Colloquium: Many-body localization, thermalization, and entanglement, Rev. Mod. Phys. **91**, 021001 (2019).

[39] P. J. Leek, J. M. Fink, A. Blais, R. Bianchetti, M. Goppl, J. M. Gambetta, D. I. Schuster, L. Frunzio, R. J. Schoelkopf, and A. Wallraff, Observation of Berry's phase in a solid-state qubit, Science **318**, 1889 (2007).

[40] J. A. Jones, V. Vedral, A. Ekert, and G. Castagnoli, Geometric quantum computation using nuclear magnetic resonance, Nature (London) **403**, 869 (2000).

[41] M. D. Schroer, M. H. Kolodrubetz, W. F. Kindel, M. Sandberg, J. Gao, M. R. Vissers, D. P. Pappas, A. Polkovnikov, and K. W. Lehnert, Measuring a Topological Transition in an Artificial Spin-1/2 System, Phys. Rev. Lett. **113**, 050402 (2014).